ADVANCED OPTICAL MATERIALS
www.advopticalmat.de

Luminescent Nd^{3+}-Based Microresonators Working as Optical Vacuum Sensors

Kevin Soler-Carracedo, Inocencio R. Martin, Marcin Runowski,* Leopoldo L. Martín, Fernando Lahoz, Antonio D. Lozano-Gorrín, and Franzette Paz-Buclatin*

Glass microspheres embedded with Nd^{3+}-doped nanoperovskites based on yttrium orthoaluminate are synthesized and used as optical vacuum sensor. Under 532 nm excitation, the microspheres show two emission bands centered at 820 and 890 nm, corresponding to the $^2H_{9/2}$,$^4F_{5/2} \rightarrow {}^4I_{9/2}$ and $^4F_{3/2} \rightarrow {}^4I_{9/2}$ transitions. When the microspheres are heated by laser excitation in air (ambient conditions), the positions of the Stark level transitions shift toward red or blue spectral regions. Additionally, the full width at half maximum of these peaks increases. Furthermore, due to the specific geometry of the microspheres, it is possible to trap the emitted light inside the microsphere resonator, in the form of whispering-gallery-modes (WGM). When the microspheres are heated, these resonant modes present higher shifts toward lower energies than those for the Stark levels. As pressure decreases, the thermal exchange (convection process) between the microsphere and the surrounding air molecules decreases, which leads to an increase on the temperature of the microsphere. Based on this effect, the response of the WGM spectral positions as a function of pressure level is used to calibrate the luminescent microspheres as optical vacuum sensors. Relative sensitivity and limit of detection are obtained and compared with other optical vacuum sensors.

1. Introduction

Vacuum technology has become an imperceptible but fundamental part of modern life. It can be found in a variety of ways from daily life uses to industry, passing through medicine or atomics physics.[1,2] The applications of vacuum technology are wide, as different operating vacuum ranges can be achieved. They can be classified either by the physical situation or by the fields where the application belongs to. However, a fundamental part of this technology is the requirement of precise and reliable vacuum measurements. The advances in the field come along with harder requirements to meet in terms of precision and miniaturization of the sensors.[3] Vacuum gauges currently used are based on mechanical deformation,[4,5] thermal conductivity[6–8] such as Pirani,[9] thermocouple or thermistor gauges; ionization[10,11] and spinning rotations.[12] All these approaches are more or less suitable depending on the pressure range of the measurements. But for all ranges, the vacuum gauges based on the previous parameters have an uncertainty from around 1% to 20%. Another approach to measure vacuum that has been barely investigated is the use of optical sensor. Up to date, the only researches following this approach were based on heterodyne[13,14] and optical fiber interferometry,[15,16] resonance effects[17–19] or magneto-optical trapping.[2]

Furthermore, luminescent materials play an important role as phosphors, contrast agent, labels, optical heaters/coolers, temperature and pressure sensors, etc.[20,21] In the field of luminescent materials, the lanthanide based organic and inorganic compounds are of special importance. This is mostly due to their favorable optical properties, such as multicolor emission and up-conversion luminescence, narrow absorption and emission bands, large Stokes shift, long radiative lifetimes, etc.[22–24]

Recently, in our previous publication,[21] we showed for the first time the possibility of converting luminescence thermometer into the optical vacuum sensor. To present this

K. Soler-Carracedo, Dr. I. R. Martin, Dr. L. L. Martín, Dr. F. Lahoz, F. Paz-Buclatin
Departamento de Física
Universidad de La Laguna
Av. Astrofísico Francisco Sánchez
s/n, La Laguna, Tenerife 38200, Spain
E-mail: ksolerca@ull.edu.es

Dr. I. R. Martin, Dr. A. D. Lozano-Gorrín
Instituto Universitario de Materiales y Nanotecnología (IMN)
Universidad de La Laguna
Santa Cruz de Tenerife
Tenerife 38200, Spain

The ORCID identification number(s) for the author(s) of this article can be found under https://doi.org/10.1002/adom.202000678.

DOI: 10.1002/adom.202000678

Dr. M. Runowski
Faculty of Chemistry
Adam Mickiewicz University
Uniwersytetu Poznańskiego 8, Poznań 61-614, Poland
E-mail: runowski@amu.edu.pl

Dr. F. Lahoz
Instituto Universitario de Estudios Avanzados en Atómica Molecular y Fotónica (IUdEA)
Universidad de La Laguna
Santa Cruz de Tenerife
Tenerife 38200, Spain

Dr. A. D. Lozano-Gorrín
Departamento de Química
Universidad de La Laguna
Av. Astrofísico Francisco Sánchez
s/n, La Laguna, Tenerife 38200, Spain

concept we used YVO_4:Yb^{3+}-Er^{3+} inorganic material, working as up-converting phosphor, luminescence thermometer and heater under NIR (975 nm) laser irradiation. Using the ratiometric technique, known as fluorescence intensity ratio (FIR) or luminescence intensity ratio (LIR) (band ratio of Er^{3+} thermally-coupled levels), and changing pressure in the system, we were able to optically determine the local temperature alterations. Correlating the local temperature and the applied pressure values, we developed the first luminescent vacuum sensor, working in the range from about $\approx 10^{-5}$ to 10^{-2} bar.

In this paper, a novel optical vacuum sensor based on Nd^{3+}-doped microspheres, and a contactless detection of whispering-gallery-modes (WGM) is presented. There exists an increasing scientific interest in WGM optical sensing. In particular, it has been reported in the literature, that WGM based temperature sensors can improve the resolution limit by orders of magnitude when compared to sensors based on the FIR technique.[25–27] By enhanced light-to-heat conversion in vacuum, thermal vacuum sensing was achieved analyzing the optical properties of transparent microspheres. Yttrium orthoaluminate nanoperovskite (YAP) was selected as a host material due to its favorable mechanical properties and chemical stability, and, most importantly, due to its appealing thermal properties; that include high thermal conductivity and thermal variation of the refractive index.[28] The nanoperovskites were doped with Nd^{3+}, that is a common dopant ion for temperature sensing,[29–32] exhibiting several radiative transitions from the thermally coupled energy levels (TCLs) $^4F_{5/2}$ and $^4F_{3/2}$. Furthermore, they can be excited with low-cost diode laser (e.g., 532 nm) and exhibit well separated bands in the 800–1000 nm range. This spectral range coincide with regular (silicon) CCD detectors response, and also with the "near-infrared biological windows" of human tissue, which is critical for diverse biological and medical applications. The nanoperovskite doped with Nd^{3+} were combined with a soda-lime glass to obtain the microsphere resonators. The fabrication method used, led to highly transparent microspheres. These microspheres were not coupled to any fibers or substrates, which is important to avoid geometrical irregularities that affect the WGM. The use of microspheres instead of a mixture of particles also presents several advantages in terms of their application for sensing devices, as microspheres can be easily and precisely manipulated with a needle or with a laser, by using the optical tweezers technique.[33,34] After temperature calibration, the microspheres were pumped at constant laser power, and their emission was recorded as a function of vacuum. Given that the emission is related to the microsphere's temperature, it is possible to calibrate them as vacuum sensors following the thermal exchange via convection process, related to the ultralow pressure in a vacuum chamber. Therefore, despite the wide use of WGM for temperature, refractive index or mass detection, among others; and despite of existing preceding works in the literature where lanthanide ions have been used for pressure sensing.[35–38] This is the first time, in the best of our knowledge, that WGM is used for vacuum sensing. The proposed method of using easy to manipulate microspheres for vacuum sensing, with improved pressure resolution in the ultralow pressure range, could lead to important new applications in nanotechnology, materials science, catalysis, medical and space technology.

2. Theoretical Background

2.1. Technique

A soda-lime glass microsphere doped with Nd^{3+} was irradiated at constant power (3 mW) and the emission was recorded as a function of vacuum. Emission changes when surrounding pressure decreases are related to temperature increment in the microsphere. Consequently, it is possible to characterize the Nd^{3+} doped microspheres as an optical vacuum sensor. Following this line of thought, a study of the different responses of the sample with temperature was made, in order to determine the best spectroscopic parameter for vacuum sensing.

One of the main techniques for optical sensors is the FIR. This technique uses the many pair of energy levels with small energy separation, in the order of the thermal energy (<2000 cm^{-1}), that can be found in various lanthanide (Ln^{3+}) doped materials. The small energy gap allows thermalization processes to occur and thus, the temperature can be estimated by the analysis of the band intensity ratio, associated with the excited TCLs of the Ln^{3+} ions involved.

For Nd^{3+} ions, the relative population between the levels can be described as a three level system that follows a Boltzmann type distribution[39]

$$\Delta(T) = \frac{I_{31}}{I_{21}} = \frac{\omega_{31}^R g_3 h\nu_3}{\omega_{21}^R g_2 h\nu_2} \exp\left(\frac{-E_{32}}{k_B T}\right) = C \exp\left(\frac{-E_{32}}{k_B T}\right) \quad (1)$$

where I_{31} and I_{21} are the emission intensities of the transitions from level 3 to 1 and level 2 to 1, respectively; k_B is the Boltzmann constant, E_{32} is the energy gap between the two thermalized excited levels 2 and 3, g_3 and g_2 are the degeneracies ($2J + 1$) of these levels, ν_3 and ν_2 are the frequencies of the transitions from level 3 and 2 to ground state respectively and ω_{31}^R and ω_{21}^R are the spontaneous emission rates from the respective levels to the ground state (E_1) and C is the pre-exponential factor. As it can be seen from Equation (1), the FIR technique is independent of the incident pump-power source, as it affects only the intensity of both emissions bands, but not their intensity ratio, that is only dependent on the temperature.

Furthermore, due to the nanocrystalline nature of the sample and the low point symmetry of the Nd^{3+} sites in the $YAlO_3$ structure, there is a complete breakdown of the neodymium energy levels leading to the rise of Stark splitting, into the crystal-field levels[40,41] It is possible to study the spectral dependence of these Stark levels, associated with the Nd^{3+} transitions, with temperature. Taking advantage of the sharpness of the narrow emission bands, corresponding to these Stark levels, it is possible to achieve the well-resolved spectra, leading to high temperature and pressure resolution. Recording these peaks as a function of temperature, it is possible to analyze the spectral shift of these peaks, as well as the evolution of their full width at half maximum (FWHM).[42]

Finally, due to the unique geometry of the microspheres, it is possible for the emitted light to get trapped inside the resonator in the form of WGM.[43] The spectral position of these WGM can be approximated to equation[44]

$$m\lambda_m = 2\pi n_{eff} R \quad (2)$$

where m is the mode number, λ_m are the resonant wavelengths, n_{eff} is the effective refractive and R the radius of the microsphere. From Equation (2), it follows that temperature changes on the microsphere will affect the spectral position of the resonant wavelengths, due to changes in n and R, described by the thermo-optic and expansion coefficients. In the case of soda-lime glass, these coefficients are both positives and so, a redshift is expected when heating the microsphere. Given the high Young modulus of soda-lime glass (5.43×10^8 Torr), it can be assumed that in the range of pressure used for the experiments (3.8 to 2.3×10^{-2} Torr), the microspheres did not suffer any significant volume strain.

2.2. Sensitivity

To characterize the sensing capability of a material, it is a common approach to use the absolute sensitivity (S), described by the rate of change of the sensing parameter as a response to the desired physical property. It is given by the formula

$$S = \left| \frac{dM_p}{dT} \right| \tag{3}$$

where M_p is the measured parameter.

However, this feature cannot be considered as a standard for comparison, as it depends on the nature of the sensing parameter and the experimental setup among others. Thus, in order to compare different sensors, Collins et al.[45] defined another figure of merit called the relative sensitivity (S_r) given as

$$S_r = \frac{1}{M_p} \left| \frac{dM_p}{dT} \right| \tag{4}$$

which allows comparison of optical sensors, even if they use different physical parameters to detect a certain change.

Another important parameter used to characterize the sensor is the limit of detection (δM_{pmin}), also known as uncertainty (sensing resolution). This parameter is related to the minimum parameter change that the sensor is capable to recorded and it is given as

$$\delta M_{p\,min} = \frac{1}{S_r} \frac{\delta M_p}{M_p} \tag{5}$$

where $\delta M_p / M_p$ is the resolution limit or relative uncertainty of the thermometric parameter, this is, the smallest change that can be experimentally detected. The resolution limit is related to the sensor performance but it is also dependent on the experimental setup.[46] Therefore, one way of improving the resolution limit could be the use of better acquisition systems, and also by configuring the measurements with longer integration time and averaging consecutive measurements to decrease experimental noise. However, such procedure increases the temporal response of the sensor, and delays determination of the measured function, which may be undesired in some applications.

3. Experimental Section

3.1. Sample Preparation

Nanocrystalline YAP perovskites of composition $Y_{(0.975)}Nd_{0.025}AlO_3$ (YAP: Nd^{3+} 2.5%) were successfully synthesized by the Pechini citrate sol–gel method in an air atmosphere. Stoichiometric molar ratios of high-purity $Y(NO_3)_3{\cdot}4H_2O$ (ALDRICH, 99.9%), $Al(NO_3)_3{\cdot}9H_2O$ (ALDRICH, 99.9%) and $Nd(NO_3)_3{\cdot}H_2O$ (ALDRICH, 99.9%) materials were dissolved in 25 mL of 1 M HNO_3 under stirring at 353 K for 3 h. Then citric acid, with a molar ratio of metal ions to citric acid of 1:2, was added to the solution, which was stirred and heated at 363 K until reaching the transparency of the solution. Then, 4 mg of polyethylene glycol was added to the solution. This last step created a gel that was fired at 400 °C for 6 h in order to remove the residual nitrates and organic compounds and the subsequently obtained powder sample was finally burnt out at 1200 °C for 20 h. The second thermal treatment was performed at 1550 °C for 12 h. The relatively high Nd^{3+} concentration (2.5 mol%) was chosen because the materials heat up more when they contain higher concentration of the optically active ions, mainly due to the enhanced cross-relaxation processes, leading to the improved light-to-heat conversion efficiency.[21]

To obtain the microspheres, a Knittel Glaser microscope slide was crushed and the grounded to a fine powder with an agate mortar. The soda lime glass powder from the slide was combined with nanoperovskites using 5 wt% of nanoperovskite versus 95 wt% of soda lime. Lastly, the resulting mixture was dropped over a horizontal butane flame. The low melting point of soda-lime glass allowed the butane flame to produce liquid glass droplets from the mixture, which turned into spheres by high surface tension during the cooling process (**Figure 1**). Transparent microspheres with diameter of around 40–50 ± 1 μm were selected (Diameter size distribution of the microspheres can be seen in Figure S1 in the Supporting Information). Note that soda-lime glass is by far the most common

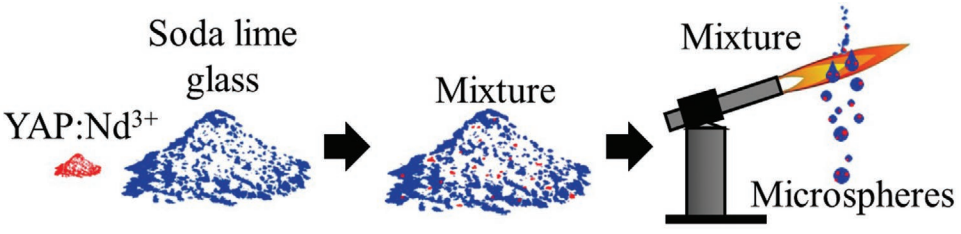

Figure 1. Schematic representation of the procedure followed to obtain the soda-lime glass microspheres doped with YAP:Nd^{3+} nanoperovskite.

and inexpensive type of glass in the market at the present time. Its low melting point make it extremely easy to work with and facilitates the melting process, required to create the microspheres by surface tension during the cooling process.

3.2. Optical Characterization

The emission spectra were obtained by exciting the material with a continuous-wave 532 nm diode pumped solid state laser (laser power fluctuation is included in Figure S2 in the Supporting Information). A modified confocal microscope was used for excitation and detection. The light was collected from the objective and focused on the entrance slit of a grating spectrometer (Andor SR-500i-B2) coupled to a CCD (Newton 970EMCCD) detector. The use of an adjustable mirror allowed, combined with the entrance slit that was narrowed to 60 µm and acted as an image plane pinhole, to partially detect the emission from one edge or the center of the microsphere image.[47] All spectra were corrected from the spectral response of the equipment. To obtain the spectral resolution of the system, the width of a single mode laser line at 532 nm was measured, resulting in a spectral resolution of about 140 pm in good agreement with the manufacturer specifications. For the resolution limit, 100 measurement of a laser profile under the same conditions were recorded. The spectra were fitted to a Gaussian curve and the uncertainty was calculated as the standard deviation of the laser peak position distribution. A standard deviation of 3 pm was obtained. Similar procedure was carried out to obtain the uncertainty of the spectral position of the Stark peaks, FWHM and WGM. For the spectral position and the FWHM evolution of the Stark peaks, 100 measurements were carried out at room temperature (RT) and ambient pressure from a single peak. A statistical study was carried out on the measurements. From this analysis, standard deviations of 7.8 and 16.7 pm were obtained for the spectral position and the WFHM, respectively. The error bars corresponding to these parameters were taken as the double of those standard deviations. To determine the uncertainty of the spectral position of the WGM, a microsphere was located inside the vacuum chamber. The 100 measurements were carried out at 3.75 Torr and 318 K. The statistical analysis from the results gave a standard deviation of 5.7 pm (see Figure S3 in the Supporting Information). The error bars in the figures that represent the spectral position of WGM corresponds to a deviation of +/− the double of the uncertainty. This way, all the possible aspects that affect the experimental setup are taken into account. These aspects include laser fluctuations, the vibrations of the optical table and the temperature fluctuations of the laboratory.

To calibrate the optical response of the sample with temperature, luminescence measurements were carried out from 293 RT to 530 K in a tubular electric furnace (Gero RES-E 230/3), where the temperature of the sample was controlled via a type K thermocouple.

Finally, the microspheres were located inside a vacuum chamber. The vacuum was obtained by an oil pump (Edwards RV3), where the pressure gauge was connected to a digital controller (Edwards Active Gauge Controller Single Display).

4. Results and Discussion

4.1. Optical Thermal Response

The emission spectrum of the glass microspheres incorporating YAP:Nd^{3+} nanoperovskites, under 532 nm excitation at RT is depicted in **Figure 2**a, showing two emissions bands corresponding to the $^2H_{9/2}$,$^4F_{5/2} \rightarrow {}^4I_{9/2}$ and $^4F_{3/2} \rightarrow {}^4I_{9/2}$ Nd^{3+} transitions at 820 and 890 nm, respectively. The small energy gap between the $^2H_{9/2}$,$^4F_{5/2}$ and $^4F_{3/2}$ levels allows thermalization processes to occur, and thus it is possible to measure the intensity ratio of both emission bands as a function of temperature using the FIR technique.

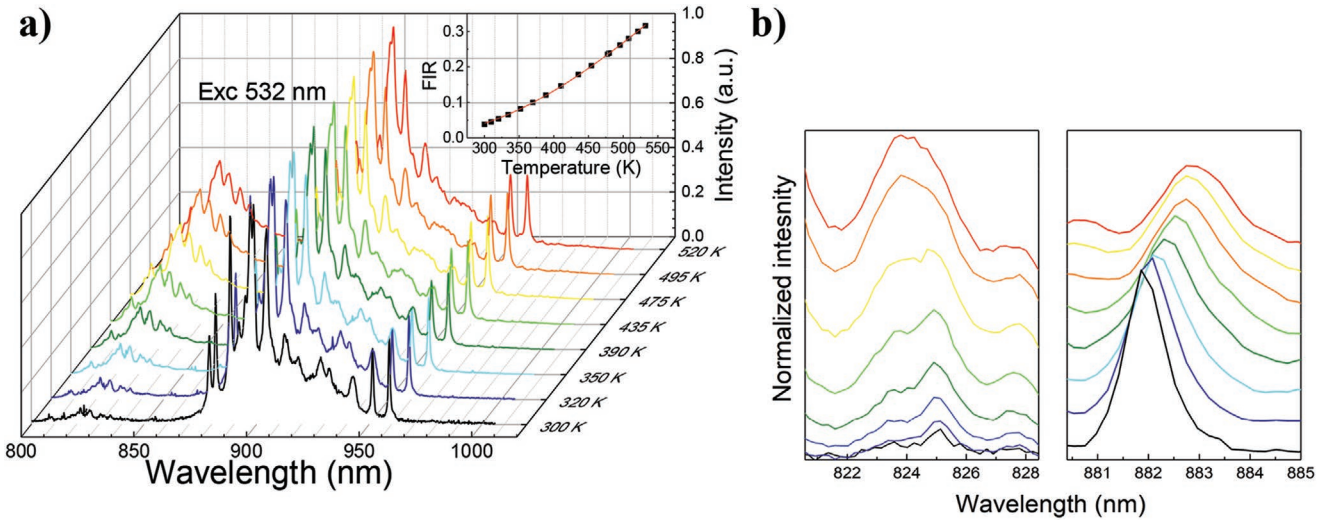

Figure 2. a) Emission spectra of the microspheres incorporated with YAP:Nd^{3+} nanoperovskites, recorded under 532 nm excitation as a function of temperature. The inset in the figure shows the FIR data fitted to Equation (1). b) Zoom at 824 and 882 nm showing the transition to the Stark levels spectral shift and FWHM change as a function of temperature.

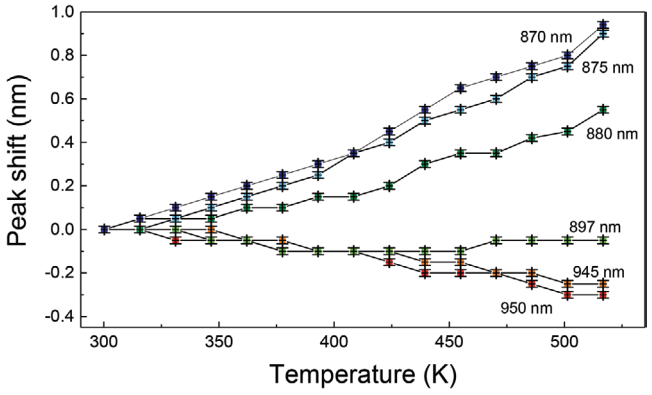

Figure 3. Peak shifts of the $^4F_{3/2}(R_{1,2}) \rightarrow {}^4I_{9/2}(Z_{1\text{-}5})$ Nd^{3+} Stark level transitions as function of temperature.

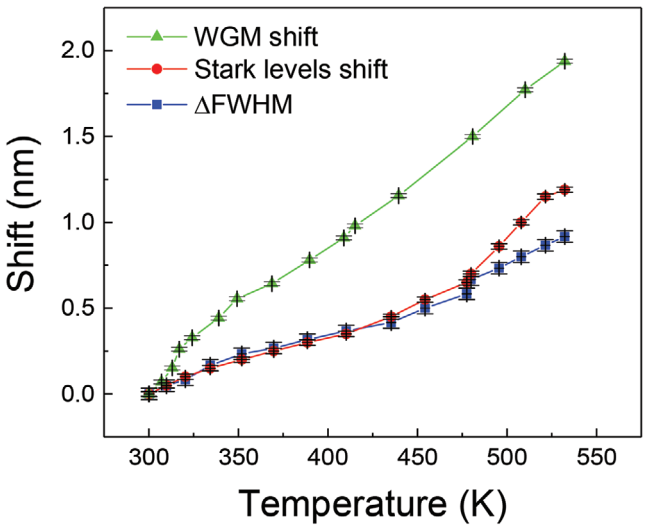

Figure 4. Mean spectral shift of WGM (green, triangles), spectral position of the Nd^{3+} Stark level transition centered at 870 nm (red, circles) and mean increment of the FWHM (blue, squares) as a function of temperature.

The appearance of sharp peak profiles is due to the low point symmetry of the Nd^{3+} sites in the $YAlO_3$ crystalline structure, which results in a breakdown of Stark levels in the mentioned levels ($^2H_{9/2}$, $^4F_{5/2}$, $^4F_{3/2}$, and $^4I_{9/2}$), corresponding to Stark levels $T_{(1\text{-}5)}$, $S_{(1\text{-}3)}$, $R_{(1,2)}$ and $Z_{(1\text{-}5)}$, respectively.[48] The appearance of these Stark levels indicates that the YAP nanoperovskites have been successfully incorporated into the microspheres structure.

In order to correlate luminescence properties of the microspheres with temperature, the sample was heated inside a tubular furnace and irradiated at 532 nm with low laser power (3 mW), in order to avoid laser heating processes. The selected temperature range, between 300 and 530 K, it is due to the correlation of the heating of the microspheres in the pressure range used for vacuum sensing (medium vacuum range). This topic will be discussed in the Optical pressure response section. As temperature increased, the band intensity ratio (FIR) changed for the 820 and 890 nm emission bands, corresponding to the $^2H_{9/2}$,$^4F_{5/2} \rightarrow {}^4I_{9/2}$ and $^4F_{3/2} \rightarrow {}^4I_{9/2}$ transitions (Figure 2a). In the inset of Figure 2a) it can be seen the corresponding FIR response of the sample from RT to 530 K, fitted to Equation (1), providing the value of energy difference between the TCLs, $E_{32} = 970\ cm^{-1}$. This value is in good agreement with the literature.[49–51]

When compared to other Nd^{3+} optical thermometers working with the same TCLs, only strontium barium niobate (SBN) glass ceramic samples showed a similar rate of change for the FIR in the selected temperature range.[49] Whereas phosphate glasses,[50] doped optical fibers[51] and fluorotellurite glasses[52] present a lower response. FIR relative sensitivity and further comparison with other optical temperature sensors can be found in Figure S4 and Table S1 in the Supporting Information.

Furthermore, the spectral position of the peaks centroids, corresponding to the $^4F_{3/2}(R_{1,2}) \rightarrow {}^4I_{9/2}(Z_{1\text{-}5})$ Nd^{3+} transitions between the Stark levels, changed as a function of temperature as well (see Figure 2b). For shorter wavelengths (870–880 nm), a red-shift to lower energies was observed, whereas for longer wavelengths (897–950 nm), shift toward higher energies was observed (see **Figure 3**). A similar behavior was observed by Hernández-Rodríguez et al.[53] when studying the effects of pressure in YAP:Nd^{3+} nanoperovskite, part of the Stark levels (from the same band) was red shifted and a second part blue-shifted. The error bars used for the spectral shift corresponds to the double uncertainty value, as it was described in the previous sections. For the temperature error bars, the standard error for a type-K thermocouple was used.

The evolution of the FWHM as a function of temperature can also be used to sense temperature variations.[42] **Figure 4** presents the spectral position shift and ΔFWHM, for the Stark level transition corresponding to the 870 nm emission, calibrated as a function of temperature from RT up to 530 K. For a clear comparison, we also included there the WGM shift, which will be discussed in the next paragraph. The error bars used for the spectral shift were obtained as it is described in the previous section, whereas for the horizontal axis it is the standard error for a type-K thermocouple.

In order to measure the WGM emission, the detection of the confocal microscope was set to an edge of the microsphere. This procedure allowed to selectively detect the emitted resonant light trapped inside the transparent cavity in the form of WGM resonance. When this was made, a series of narrow peaks (sharper than the Stark level transitions) corresponding to the WGM appeared, superimposed to the emission spectrum (**Figure 5**a). The microsphere was then laser-heated (by increasing the incident pump power), and the local temperature values were determine using the previously done calibration, based on the FIR technique. When heating the microsphere, the spectral position of the WGM exhibit a red shift due to the thermal heating produced by the laser, as it was expected due to the positive thermo-optic and expansion coefficients of the glass microspheres. The spectral position of four WGM, corresponding to $m = 312$, 311, 310, and 309 obtained from Equation (2) with $R = 30$ µm and $n_{eff} = 1.52$, obtained by increasing the temperature from RT up to 530 K can be seen in Figure 5b.

Comparing the mean WGM shift (shown in Figure 4) with the peak shift and the ΔFWHM for the Stark level transition at 870 nm, all as a function of temperature, the WGM temperature response was much more sensitive in the measured range. In the range from RT to 530 K, the highest Stark level shift and

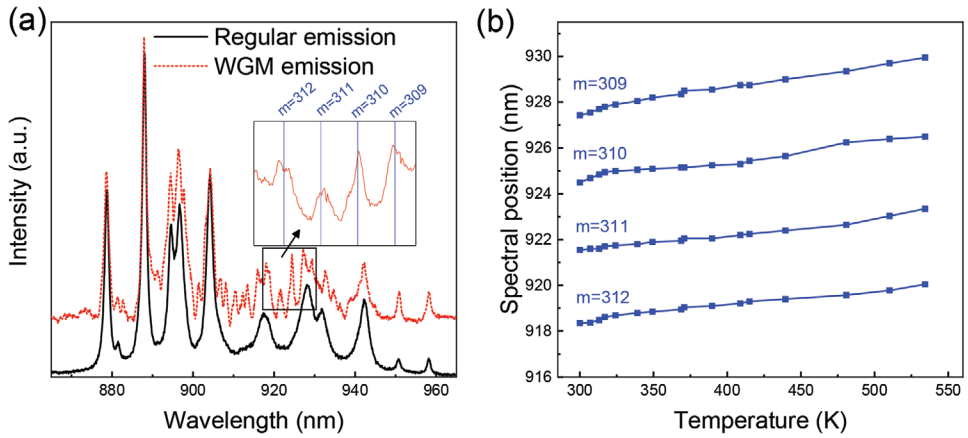

Figure 5. a) Emission from crystalline YAP nanoperovskites doped with Nd^{3+} in powder (black, continuous line) and microsphere presenting WGM (red, dashed line). b) WGM spectral position as a function of temperature. The inset in (a) shows the fitting of the experimental data to Equation (5) for the 4 selected WGM.

FWHM variation was about 0.9 nm, whereas the spectral position of the WGM changed by ≈2 nm. Moreover, while the spectral positions of the transition between Stark levels shift toward different energies with respect to the selected wavelength, WGM response with temperature is only related to the thermo-optic and expansion coefficient, so only a red-shift of the WGM is observed. As these resonant modes share the same behavior, facilitating the calibration, it is possible to measure the shift of the multiple peaks to minimize detection errors.[46]

4.2. Optical Pressure Response

Following these results, the investigated microspheres were located inside a vacuum chamber, and excited with a 532 nm laser, resulting in the appearance of many WGM in the spectrum. The spectra were recorded in the pressure range from ≈3.8 to 2.3×10^{-2} Torr (medium vacuum range). It was not possible to calibrate the sensor for pressures below 2.3×10^{-2} Torr due to technical limitations of our vacuum system. As the pressure decreased, a reduction of the thermal exchange (convection process) between the microsphere and the surrounding air molecules was expected. Therefore, the temperature of the microsphere increases, producing red-shift of the WGM peaks. **Figure 6** shows a schematic representation of the experiment and the microsphere resonator used, emphasizing the behavior of the WGM in air and under vacuum conditions.

The mean shift of the spectral position for four different resonant modes as a function of vacuum is presented in **Figure 7**. The associated local temperature change, obtained from FIR calibration, is also presented in the top axis of the same figure.

For a pressure range from 3.8 to 2.3×10^{-2} Torr, the spectral position of the WGM had a total shift of about 4 nm. Similarly to Runowski et al.,[21] when pressure decreases below 1–2 Torr, an increase in the response of the sensor can be observed. With a rate change of ≈0.26 to 1 nm $Torr^{-1}$. The error bars from the WGM shift correspond to the double uncertainty value that is described in the "Optical characterization" section. Note, that it is a constant value for all the pressure range and it is due to the logarithmic scale that it seems to increase for pressures closer to 3.75 Torr. For the pressure error bars the manufacturer specifications were used: 0.1, 0.01, and 0.001 Torr for the 10^0, 10^{-1} and 10^{-2} Torr ranges, respectively.

Based on the spectral positions of the WGM as a function of pressure (Figure 7), the relative sensitivity of the sensor was evaluated with the following equation

$$S_r = \frac{1}{M_p}\left|\frac{dM_p}{dP}\right| \tag{6}$$

where M_p is the shift of the WGM.

As it was expected, the relative sensitivity increased for lower pressures, reaching a maximum value of almost 12% $Torr^{-1}$ at 2.3×10^{-2} Torr (**Figure 8**).

To determine the limit of pressure detection from Equation (5), 100 measurements were carried out with the microsphere placed in the vacuum chamber, at pressure

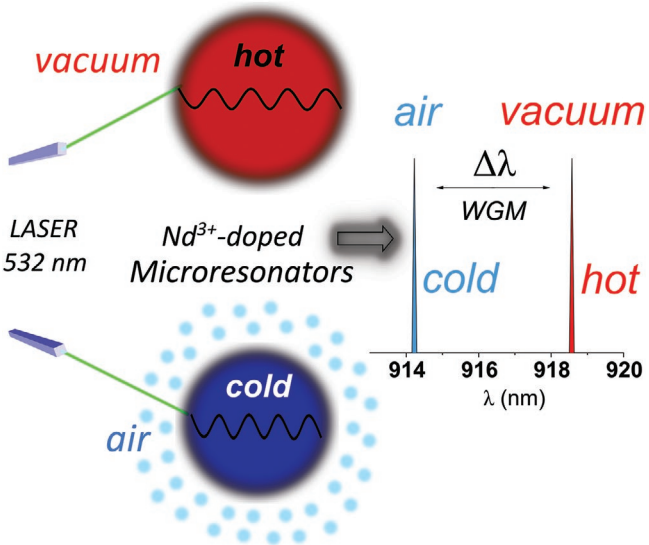

Figure 6. Schematic representation of the vacuum sensor based on WGM spectral shift for Nd^{3+}-based microspheres.

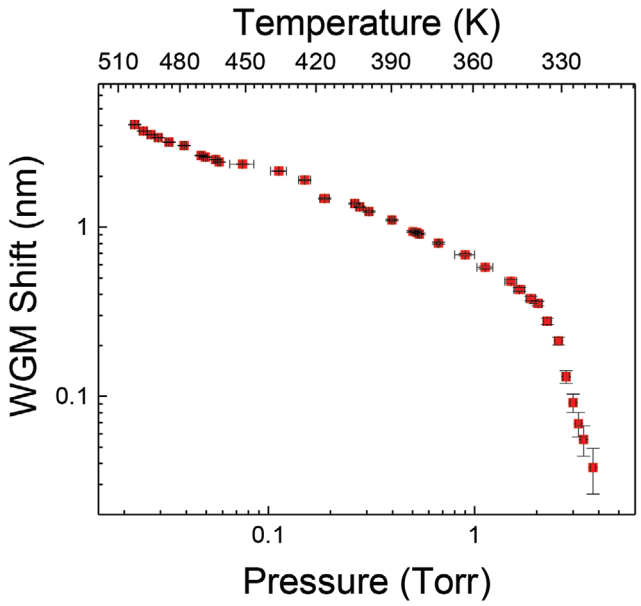

Figure 7. WGM spectral shift for the Nd^{3+}-based microspheres as a function of vacuum.

3.75 Torr. The spectral position of WGM were analyzed for all measurements and, the resolution limit was taken as the standard deviation of the statistical distribution ($\sigma = 5.7 \times 10^{-3}$ nm). The resulting limit of detection presented a minimum of 5.3×10^{-5} Torr at 2.3×10^{-2} Torr and a maximum of 4.19×10^{-2} Torr at 3.75 Torr, corresponding to the pressure resolution from ≈0.24% to 1.1%, respectively. Most vacuum gauges based on thermal conductivity,[54] viscosity of gases[55] or mechanical deformation[56] present similar performance, with uncertainties around 1% when measuring over 0.1 Torr. For values under 0.1 Torr, the spinning rotator scheme is usually adopted for vacuum sensing. This scheme presents uncertainties up to 10% at pressures close to 10^{-2} Torr, while the limit of detection of microspheres incorporating nanoperovskites doped with Nd^{3+} goes down to values around 0.24%. In other words, the pressure resolution of our vacuum sensor is significantly higher, allowing much more accurate measurements in the mentioned pressure range.

The new sensor showed an improvement, in terms of limit of detection when compared to the previous YVO_4:Yb^{3+}-Er^{3+} inorganic material.[21] At 7.5×10^{-1} Torr, this sensor presents a pressure resolution of 1.1×10^{-2} Torr whereas YVO_4:Yb^{3+}-Er^{3+} has 1.9×10^{-2} Torr. For lower pressure, the improvement is more significant with a limit of detection of 6.3×10^{-4} Torr at 7.5×10^{-2} Torr for this sensor, against the 1.5×10^{-3} Torr of its predecessor. Now, to compare to other optical vacuum gauges found in the literature, not many works can be found that include relative sensitivity and/or limit of detection results. Uttamchandani et al.[17] presented a sensor, based on resonant diaphragm vibrations, capable of covering from 0 to 560 Torr with a relative sensitivity of 0.03% $Torr^{-1}$. Values similar to the relative sensitivity obtained in this work in the range where the sensitivity decays. Chiang et al.[14] reported a sensor based on heterodyne interferometry, with a working range from 10 to 760 Torr. There are not relative sensitivity values presented in that work, as the sensor was analyzed in terms of absolute sensitivity given in phase degree divided by Torr, which cannot be compared to other sensors based on the response of different physical phenomena. However, they present uncertainty values from 0.4% to 2.6%, as pressure increases and claim to have improved the previous work based on the same principle by Chiu et al.,[13] with a working range from 0.1 to 760 Torr, but with a minimum limit of detection of 0.5%. Our glass microspheres incorporated with Nd^{3+}-doped nanoperovskites presents uncertainties one order of magnitude lower (≈10-times better resolution), in all the measured pressure range from 3.8 to 2.25×10^{-2} Torr.

5. Conclusions

In summary, microresonators based on the glass microspheres incorporating YAP:Nd^{3+} nanoperovskites were obtained and used as optical, luminescent vacuum sensor. Stark level transitions and luminescent whispering-gallery-modes (WGM) were recorded as a function of temperature. The variation of FWHM, spectral positions for the Stark level transitions and

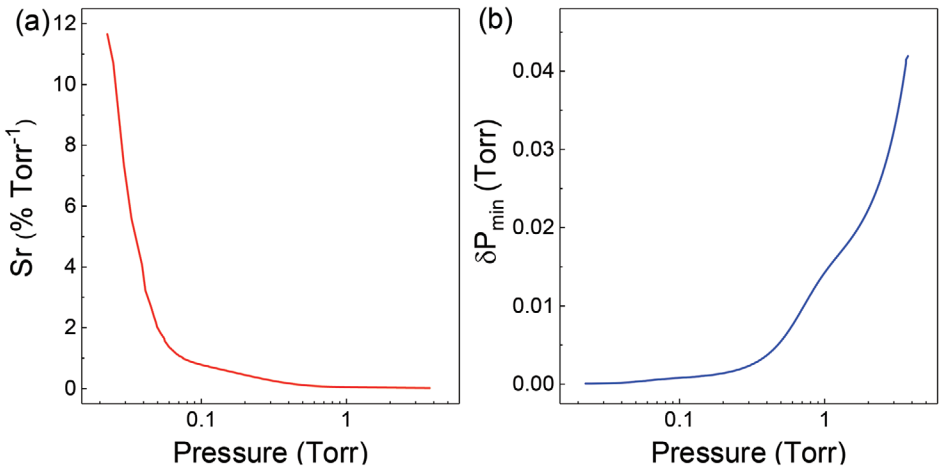

Figure 8. a) Relative sensitivity and b) limit of detection (pressure resolution) of the sensor, based on the WGM spectral shift.

for the WGM were determined. The WGM spectral shift was almost twice higher (more sensitive) compared to the other parameter changes. In view of this result, a microsphere resonator was located inside a vacuum chamber and irradiated with 532 nm laser, resulting in the appearance of very sharp WGM in the spectra. Due to the laser-induced heating of the material in vacuum conditions, the WGM spectral positions were correlated with pressure and calibrated as a vacuum sensor. A spectral shift of 4 nm was observed for a pressure change from 3.8 to 2.3×10^{-2} Torr. Relative sensitivity and limit of detection were calculated and compared to the literature. The developed sensor presented higher sensitivity and lower limit of detection than other optical vacuum sensors. Among other advantages, this sensor includes contactless localized measurement in the "near-infrared biological window", as well as miniaturization capability and low cost diode laser as excitation. Making YAP:Nd^{3+} nanoperovskites a promising candidate for vacuum sensing applications, in situations where conventional pressure gauges are impractical due to constrains in the vacuum system design. All of this advantages entails a big step forward for the modern ultralow pressure sensing in micron-sized areas.

Further work could include calibration at different laser powers, as previous works have proved that the increase in laser power can improve the sensor responsivity. A more precise vacuum setting could also be used in order to study the operating range limits of the sensor.

Supporting Information

Supporting Information is available from the Wiley Online Library or from the author.

Acknowledgements

The authors wish to thank financial support from MINECO and AEI (MAT2016-79866-R, MAT2016-75586-C4-4-P, FIS2017-82855-P, PID2019-107335RA-I00, PID2019-110430GB-C21, PID2019-106383GB-C44), AEI (IJCI-2016-30498) and EU-FEDER. M.R. is a recipient of the Bekker Programme scholarship supported by the Polish National Agency for Academic Exchange.

Conflict of Interest

The authors declare no conflict of interest.

Keywords

lanthanide ions, light-to-heat conversion, luminescence pressure sensing, microspheres resonators, whispering-gallery-modes (WGM)

Received: April 22, 2020
Revised: June 21, 2020
Published online: July 14, 2020

[1] A. Roth, *Vacuum Technology*, Elsevier, Amsterdam **2012**.
[2] T. Arpornthip, C. A. Sackett, K. J. Hughes, *Phys. Rev. A* **2012**, *85*, 033420.
[3] N. Moelders, J. T. Daly, A. C. Greenwald, E. A. Johnson, M. P. McNeal, *MRS Proc.* **2003**, *782*, A5.32.
[4] K. Harada, K. Ikeda, H. Kuwayama, H. Murayama, *Sens. Actuators, A* **1999**, *73*, 261.
[5] J. J. Sullivan, *J. Vac. Sci. Technol., A* **1985**, *3*, 1721.
[6] R. E. Ellefson, A. P. Miiller, *J. Vac. Sci. Technol., A* **2000**, *18*, 2568.
[7] A. Berman, *Total Pressure Measurements in Vacuum Technology*, Academic Press, Orlando **1985**.
[8] J. M. Lafferty, *Foundations of Vacuum Science and Technology*, Wiley, New York **1998**.
[9] F. T. Zhang, Z. Tang, J. Yu, R. C. Jin, *Sens. Actuators, A* **2006**, *126*, 300.
[10] W. C. Schuemann, *Rev. Sci. Instrum.* **1963**, *34*, 700.
[11] C. Dong, G. R. Myneni, *Appl. Phys. Lett.* **2004**, *84*, 5443.
[12] J. K. Fremerey, *J. Vac. Sci. Technol., A* **1985**, *3*, 1715.
[13] M.-H. Chiu, J.-Y. Lee, D.-C. Su, K.-H. Lee, *Precis. Eng.* **1999**, *23*, 260.
[14] K.-H. Chiang, M.-C. Hsieh, J.-Y. Lin, *Opt. Laser Technol.* **2019**, *115*, 508.
[15] B. McMillen, C. Jewart, M. Buric, K. P. Chen, Y. Lin, W. Xu, *Appl. Phys. Lett.* **2005**, *87*, 234101.
[16] K. Totsu, Y. Haga, M. Esashi, in *TRANSDUCERS '03. 12th Int. Conf. on Solid-State Sensors, Actuators and Microsystems. Digest of Technical Papers (Cat. No.03TH8664)*, IEEE, Piscataway, NJ **2003**, pp. 931–934.
[17] D. Uttamchandani, K. E. B. Thornton, J. Nixon, B. Culshaw, *Electron. Lett.* **1987**, *23*, 152.
[18] S. Inaba, K. Hane, *Appl. Opt.* **1992**, *31*, 2969.
[19] S. Inaba, K. Hane, *J. Vac. Sci. Technol., A* **1991**, *9*, 3173.
[20] C. Feldmann, T. Jüstel, C. R. Ronda, P. J. Schmidt, *Adv. Funct. Mater.* **2003**, *13*, 511.
[21] M. Runowski, P. Woźny, S. Lis, V. Lavín, I. R. Martín, *Adv. Mater. Technol.* **2020**, *5*, 1901091.
[22] J.-C. G. Bünzli, *Trends Chem.* **2019**, *1*, 751.
[23] K. Binnemans, *Chem. Rev.* **2009**, *109*, 4283.
[24] P. A. Tanner, *Chem. Soc. Rev.* **2013**, *42*, 5090.
[25] L. L. Martín, C. Pérez-Rodríguez, P. Haro-González, I. R. Martín, *Opt. Express* **2011**, *19*, 25792.
[26] L. Labrador-Páez, C. Pérez-Rodríguez, S. Ríos, D. Alonso, J. M. Cáceres, I. R. Martín, *Sens. Actuators, A* **2015**, *233*, 422.
[27] C. Pérez-Rodríguez, L. Labrador-Páez, I. R. Martín, S. Ríos, *Laser Phys. Lett.* **2015**, *12*, 046003.
[28] R. Moncorgé, B. Chambon, J. Y. Rivoire, N. Garnier, E. Descroix, P. Laporte, H. Guillet, S. Roy, J. Mareschal, D. Pelenc, J. Doury, P. Farge, *Opt. Mater.* **1997**, *8*, 109.
[29] G. Gao, D. Busko, S. Kauffmann-Weiss, A. Turshatov, I. A. Howard, B. S. Richards, *J. Mater. Chem. C* **2018**, *6*, 4163.
[30] P. Cortelletti, A. Skripka, C. Facciotti, M. Pedroni, G. Caputo, N. Pinna, M. Quintanilla, A. Benayas, F. Vetrone, A. Speghini, *Nanoscale* **2018**, *10*, 2568.
[31] S. Balabhadra, M. L. Debasu, C. D. S. Brites, L. A. O. Nunes, O. L. Malta, J. Rocha, M. Bettinelli, L. D. Carlos, *Nanoscale* **2015**, *7*, 17261.
[32] S. Zhou, G. Jiang, X. Wei, C. Duan, Y. Chen, M. Yin, *J. Nanosci. Nanotechnol.* **2014**, *14*, 3739.
[33] J. R. Moffitt, Y. R. Chemla, S. B. Smith, C. Bustamante, *Annu. Rev. Biochem.* **2008**, *77*, 205.
[34] S. Kaminski, L. L. Martin, T. Carmon, *Opt. Express* **2015**, *23*, 28914.
[35] A. Lay, C. Siefe, S. Fischer, R. D. Mehlenbacher, F. Ke, W. L. Mao, A. P. Alivisatos, M. B. Goodman, J. A. Dionne, *Nano Lett.* **2018**, *18*, 4454.
[36] T. Zheng, M. Runowski, P. Woźny, S. Lis, V. Lavín, *J. Mater. Chem. C* **2020**, *8*, 4810.
[37] M. Runowski, A. Shyichuk, A. Tymiński, T. Grzyb, V. Lavín, S. Lis, *ACS Appl. Mater. Interfaces* **2018**, *10*, 17269.
[38] M. Runowski, J. Marciniak, T. Grzyb, D. Przybylska, A. Shyichuk, B. Barszcz, A. Katrusiak, S. Lis, *Nanoscale* **2017**, *9*, 16030.
[39] S. A. Wade, S. F. Collins, G. W. Baxter, *J. Appl. Phys.* **2003**, *94*, 4743.

[40] U. R. Rodríguez-Mendoza, S. F. León-Luis, J. E. Muñoz-Santiuste, D. Jaque, V. Lavín, *J. Appl. Phys.* **2013**, *113*, 213517.
[41] V. Monteseguro, M. Rathaiah, K. Linganna, A. D. Lozano-Gorrín, M. A. Hernández-Rodríguez, I. R. Martín, P. Babu, U. R. Rodríguez-Mendoza, F. J. Manjón, A. Muñoz, C. K. Jayasankar, V. Venkatramu, V. Lavín, *Opt. Mater. Express* **2015**, *5*, 1661.
[42] S. Kumari, A. Khare, *Appl. Surf. Sci.* **2013**, *265*, 180.
[43] T. Reynolds, N. Riesen, A. Meldrum, X. Fan, J. M. M. Hall, T. M. Monro, A. François, *Laser Photonics Rev.* **2017**, *11*, 1600265.
[44] K. Soler-Carracedo, A. Ruiz, I. R. Martín, F. Lahoz, *J. Alloys Compd.* **2019**, *777*, 198.
[45] S. F. Collins, G. W. Baxter, S. A. Wade, T. Sun, K. T. V. Grattan, Z. Y. Zhang, A. W. Palmer, *J. Appl. Phys.* **1998**, *84*, 4649.
[46] C. D. S. Brites, A. Millán, L. D. Carlos, in *Handbook on the Physics and Chemistry of Rare Earths* (Eds: J.-C. G. Bünzli, V. K. Pecharsky), Vol. *49*, Elsevier, Amsterdam **2016**, pp. 339–427.
[47] C. G. B. Garrett, W. Kaiser, W. L. Bond, *Phys. Rev.* **1961**, *124*, 1807.
[48] J. R. Henderson, M. Muramoto, J. B. Gruber, *J. Chem. Phys.* **1967**, *46*, 2515.
[49] P. Haro-González, I. R. Martín, L. L. Martín, S. F. León-Luis, C. Pérez-Rodríguez, V. Lavín, *Opt. Mater.* **2011**, *33*, 742.
[50] C. Pérez-Rodríguez, L. L. Martín, S. F. León-Luis, I. R. Martín, K. K. Kumar, C. K. Jayasankar, *Sens. Actuators, B* **2014**, *195*, 324.
[51] F. Sidiroglou, S. A. Wade, N. M. Dragomir, G. W. Baxter, S. F. Collins, *Rev. Sci. Instrum.* **2003**, *74*, 3524.
[52] E. A. Lalla, S. F. León-Luis, V. Monteseguro, C. Pérez-Rodríguez, J. M. Cáceres, V. Lavín, U. R. Rodríguez-Mendoza, *J. Lumin.* **2015**, *166*, 209.
[53] M. A. Hernández-Rodríguez, J. E. Muñoz-Santiuste, V. Lavín, A. D. Lozano-Gorrín, P. Rodríguez-Hernández, A. Muñoz, V. Venkatramu, I. R. Martín, U. R. Rodríguez-Mendoza, *J. Chem. Phys.* **2018**, *148*, 044201.
[54] M. v. Pirani, *Verh. Dtsch. Phys. Ges.* **1906**, *8*, 686.
[55] J. Fremerey, *Vacuum* **1982**, *32*, 685.
[56] V. H. Dibeler, F. Cordero, *J. Res. Natl. Bur. Stand.* **1951**, *46*, 1.